Applied Mathematics & Information Sciences
An International Journal

Effective Extraction of Gabor Features for False Positive Reduction and Mass Classification in Mammography

Muhammad Hussain [1,*]*, Salabat Khan*[2]*, Ghulam Muhammad*[3]*, Iftikhar Ahmad*[4] *and George Bebis*[5]

[1] Department of Computer Science, College of Computer and Information Sciences, King Saud University, Riyadh 11543, Saudi Arabia
[2] Department of Computer Science, National University of Computer and Emerging Sciences, Islamabad, Pakistan
[3] Department of Computer Engineering, College of Computer and Information Sciences, King Saud University, Riyadh 11543, Saudi Arabia
[4] Department of Software Engineering, College of Computer and Information Sciences, King Saud University, Riyadh 11543, Saudi Arabia
[5] Department of Computer Science and Engineering, University of Nevada at Reno

Abstract: Digital mammography is considered to be the most effective imaging modality for early detection of breast cancer. Masses and microcalcifications are two early signs of breast cancer. For the detection of masses, segmentation of mammograms results in ROIs (regions of interest) which not only include masses but suspicious normal tissues as well, which lead to false positives. The problem is to reduce the false positives by classifying ROIs as masses and normal tissues. In addition, the detected masses are required to be classified as malignant and benign. We address these two problems using textural properties of masses. Gabor filter bank is used in a novel way to extract the most representative and discriminative textural properties of masses present at different orientations and scales. SVM with Gaussian kernel is employed for classification. The method is evaluated over 1024 (512 masses and 512 normal) ROIs extracted from DDSM database. Experiments have been performed with different parameter settings to find the best set of parameters. Gabor filter Banks with different choices of orientations (3, 5, 6, 8) and scales (2, 3, 4, 5) have been tested on 4 ROI resolutions (64×64, 128×128, 256×256, 512×512). For the first problem i.e. to classify ROIs as masses and normal tissues, the best result (Az = 0.96±0.02) is obtained when Gabor filter bank with 5 orientations and 3 scales and RIOs with size 512×512 is used. Gabor filter bank with 8 orientations and 5 scales on mass ROIs of size 128×128 gives the best result (Az = 0.87±0.05) for the second problem (i.e. to classify mass ROIs as benign and malignant). Comparison with state-of-the-art methods reveals that the proposed method performs better than the existing methods.

Keywords: Breast cancer detection, Gabor filter bank, Directional features, Mass detection, Moments based features.

1. Introduction

Breast cancer is the major form of cancer that has fatal effects on women all over the world. According to the statistics of National Cancer Institute, Surveillance, Epidemiology, and End Results (SEER) program, lifetime risk of developing breast cancer among American women is 12.2 % (i.e. one in eight), exceeded only by lung cancer [1,2]. In the European Community, breast cancer represents 19% of cancer deaths and 24% of all cancer cases [3,4]. The World Health Organization's International Agency for Research on Cancer (IARC) estimated more than one million cases of breast cancer to occur annually and reported that more than 400, 000 women die each year from this fatal disease [5].There are three types of breast lesions: masses, calcifications and architectural disorders [2]. In this study our focus is on masses. Mammography is considered to be a reliable and effective screening method for the detection of masses. By digitizing mammograms and exploiting contemporary powerful image analysis techniques, computer aided diagnosis (CAD) systems can be developed for effectively assisting the radiologists. A CAD system consists of automatic or semiautomatic techniques developed to assist radiologists in the detection and classification of breast lesions [3]. CAD systems are easy to use tools that are inexpensive and by analyzing the digital mammograms they can effectively assist the radiologists in their decision

---

* Corresponding author e-mail: mhussain@ksu.edu.sa

making process (as a second expert opinion). The idea of using CAD system for breast cancer detection is not recent. CAD systems have been used earlier for this task and proved to be useful in the screening process of digital mammograms and the detection of early stage malignancies [2,3,5]. However, there exist controversial results and views against the usage of CAD systems mainly because of their high false positive and false negative rates in the breast cancer detection, which makes radiologists not really trust them [3]. False negative occurs when a CAD system declares a mass region in a mammogram to be normal. The main cause of the false negatives is the density of the breast, as both dense tissues and masses appear as white regions in the mammogram which makes it difficult to distinguish between them. As women get older, their breasts become fatty and false negatives are less likely to occur. A false positive is a region in the mammogram that is normal but interpreted as mass by the CAD system.

A CAD system involves three main stages: detection and segmentation, false positive reduction, and discrimination of benign and malignant masses. The detection and segmentation stage identifies potential mass regions, and detect their precise outlines. The detected ROIs by this stage include not only masses but suspicious normal tissues as well. The false positive reduction stage classifies the detected ROIs into mass and normal ROIs. The detected mass ROIs are further discriminated as benign and malignant in the final stage. Many efforts have been made so far for false positive reduction and benign-malignant classification but these are still challenging problems. In this research work, our motivation is to develop a robust and discriminative feature extraction mechanism for false positive reduction and benign-malignant classification to optimize the performance of CAD systems.

The proposed approach employs the textural properties for a robust and discriminative representation of masses. The textural properties are useful to correctly represent masses [3]. We employ Gabor filter bank in a novel way to extract the texture descriptors that characterize micro-patterns (e.g. edges, lines, spots and flat areas) at different scales and orientations. Mammograms contain texture patterns at different scales and orientations. Gabor filter bank allow different choices for the number of scales and orientations. As such, while using Gabor filter bank, an important question to address is how many scales and orientations are necessary to represent accurately the texture patterns of mass ROIs. In addition, extracted ROIs have different sizes; it is difficult to process ROIs of different sizes with Gabor filter bank. There is the need to resize ROIs. This puts another question: which size of ROIs will yield optimal results. Although, Gabor filters have been used for breast cancer detection earlier (see e.g. [2] and references therein), the features have extracted using either local or global approach. We apply Gabor filter bank specifically for false positive reduction and benign-malignant classification problems and our approach for feature extraction is taken to be a blend of local and global approaches. We divide each suspicious ROI into overlapping windows, which

form the global representation. Then, we apply Gabor filter bank on each window and extract the moments (mean, standard deviation, skewness) from the magnitudes of Gabor responses, which form the local representation of each window at different scales and orientations. The concatenation of moments of Gabor magnitude responses for all windows corresponding to an ROI is a blend of local and global feature representations. The main contributions of our work are as follows.

– For mass description, a scale and rotation invariant texture descriptor based on Gabor filter bank that is robust against noisy data.
– A new method for false positive reduction and benign-malignant classification.
– Answers to the questions: which resolution of ROIs and how many scales and orientations of Gabor filter bank yield optimal results.

The remainder of this paper is organized as follows. In the next section, we review the related research. In Section 3, we present the proposed method. Subsequently, in Section 4, we present some experimental results to show the effectiveness of the proposed technique. Finally, Section 5 concludes this work.

2. Related Work

Mass detection problem has attracted the attention of many researchers, and many techniques have been proposed so far. For a detailed review of these methods, an interested reader is referred to the review papers [17,18,19,20]. In the following paragraphs, we give an overview of the most related and recent methods.

Most of the existing methods differ in the types of features that have been used for false positive reduction and benign-malignant classification and the way these features have been extracted. Different types of features such as texture, gradient, grey-level, and shape [17] features have been employed. Texture is an important characteristic that helps to discriminate and identify the objects. In addition to other identification/detection tasks, texture descriptors have been used for detecting normal and lesion regions in mammograms [21,23]. Wei et al. [24] extracted multiresolution texture features from wavelet coefficients and used them for the discrimination of masses from normal breast tissues. They used linear discriminant analysis for classifying the ROIs as mass or non-mass. This method was tested with 168 ROIs containing biopsy-proven masses and 504 ROIs containing normal parenchyma, and resulted in Az = 0.89 (percentage area under ROC curve) and 0.86 for the training and test groups.

If texture is described accurately, then texture descriptors can perform better than other descriptors [3]. Llad et al. [4] used spatially enhanced LBP (Local Binary Pattern) descriptor, which is basically a texture descriptor, to represent textural properties of masses and to reduce false

positives; this method achieved an overall accuracy of Az = 0.94±0.02 (percentage area under ROC curve) on 512 ROIs (256 normal and 256 masses) extracted from mammograms from DDSM database. LBP based method outperforms other CAD methods for mass detection. But LBP descriptor builds statistics on local micro-patterns (dark/ bright spots, edges, and flat areas etc.) and is not robust against noise. The scheme proposed by Sampaio et al. [25] used geo-statistic functions for extracting texture features, SVM for classification and obtained the accuracy of Az = 0.87.Gabor wavelet is one of those methods which have been used for texture description in various image processing and analysis approaches [11, 26]. Gabor filters decompose an image into muple scales and orientations and make the analysis of texture patterns easy. Mammograms contain a lot of texture, and as such Gabor filters are suitable for texture analysis of mammograms [27, 28] as well. Gabor filters have been used for mass detection [2, 29].

Different texture description techniques using Gabor wavelets differ in the way the texture features have been extracted. Zheng [2]employed Gabor filters to create 20 Gabor images, which were then used to extract a set of edge histogram descriptors. He used KNN along with fuzzy c-means clustering as a classifier. The method was evaluated on 431 mammograms (159 normal cases and 272 containing masses) from DDSM database using tenfold cross validation. This method achieved true positive (TP) rate of 90 % at 1.21 false positive per image. The data set used for validation is biased toward abnormal cases which will surely favor the mass cases, and it cannot be regarded as fair evaluation. This method extracts edge histograms which are holistic descriptor, and does not represent well the local texture patterns of masses .

Lahmiri and Boukadoum [29]used Gabor filters along with discrete wavelet transform (DWT) for mass detection. They applied Gabor filter bank at different frequencies and spatial orientations on HH high frequency subband image obtained using DWT, and extracted statistical features (mean and standard deviation) from the Gabor images. For classification, they used SVM with polynomial kernel. The method was tested on 100 mammograms from DDSM database using tenfold cross validation. This method achieved an accuracy of 98]%. Though the detection accuracy is good but the size of the dataset used for testing was small. Costa et al. [30] explored the use of Gabor wavelets along with principal component analysis (PCA) for feature extraction, independent component analysis (ICA) for efficient encoding, and linear discriminant analysis (LDA) for classification. The success rate of this method with feature extraction using Gabor wavelets was 85.05 % on 5090 ROIs extracted from mammograms.

Geralodo et. al. [31]used Moran's index and Geary's coefficients for texture description and tested their approach for false positive reduction and benign-malignant classification. They obtained an accuracy of 96.04% and Az = 0.946 with Geary's coefficient and an accuracy of 99.39% and Az = 1 with Moran's index for the classification of normal and abnormal cases. For the second case (benign vs. malignant), an accuracy of 88.31% and Az = 0.804 with Geary's coefficient and accuracy of 87.80% and Az = 0.89 with Moran's index is reported. The method is tested over 1394 ROI images collected from DDSM database using tenfold cross validation. In the research work of Ioan Buciu et. al. [16], magnitude responses of 2D Gabor wavelets are investigated as features for proximal SVM. A total of 322 mammogram images from Mammographic Image Analysis Society (MIAS) database are used for three experimental cases i.e. discrimination between the three classes: normal, benign and malign (using one against all SVM classification), normal vs. tumor (benign and malign) and benign vs. malignant using 80% data for training and 20% as testing set. The dimension of the feature space of the subband corresponding to a Gabor filter is equal to the number of pixels present in the mammogram image (for a single Gabor filter). Later PCA is used to project features on a lower dimensional space. The best results (in terms of accuracy) for the three experimental cases are: 75%, 84.37% and 78.26%, respectively.

3. Materials and Methods

In this section, we present the detail of the proposed method for false positive reduction and benign-malignant classification. First, we give the detailed description of the new features extraction method; this technique is based on Gabor filter bank and is our main contribution. Then we give an overview of the classification technique used in our method.

3.1. Feature Extraction using Gabor Filter Bank

Texture is an important part of the visual world of animals and humans; they can successfully detect, discriminate, and segment texture using their visual systems [6]. Texture micro-patterns like edges, lines, spots and flat areas in an image provide different kinds of useful discriminative information. Mammograms do contain texture micro-patterns at different scales and orientations. These micro-patterns are helpful in the discrimination between mass and non-mass, and further between benign and malignant masses. Gabor filters can be used effectively to extract these micro-patterns. Since we extract texture features using Gabor filter bank, first a brief overview of Gabor filter bank is necessary for a deep understanding of the producer for feature extraction. Feature extraction procedure includes three main steps: 1) to partition each ROI into sub-regions (windows) , 2) to apply Gabor filter bank on each window separately, and 3) to compute moments (mean, standard deviation, skewness) based features from the magnitude of Gabor filter bank responses. The most computationally intensive task in our method is the feature extraction task. Fortunately, this task can be highly parallelized to achieve the better computational efficiency. A detailed
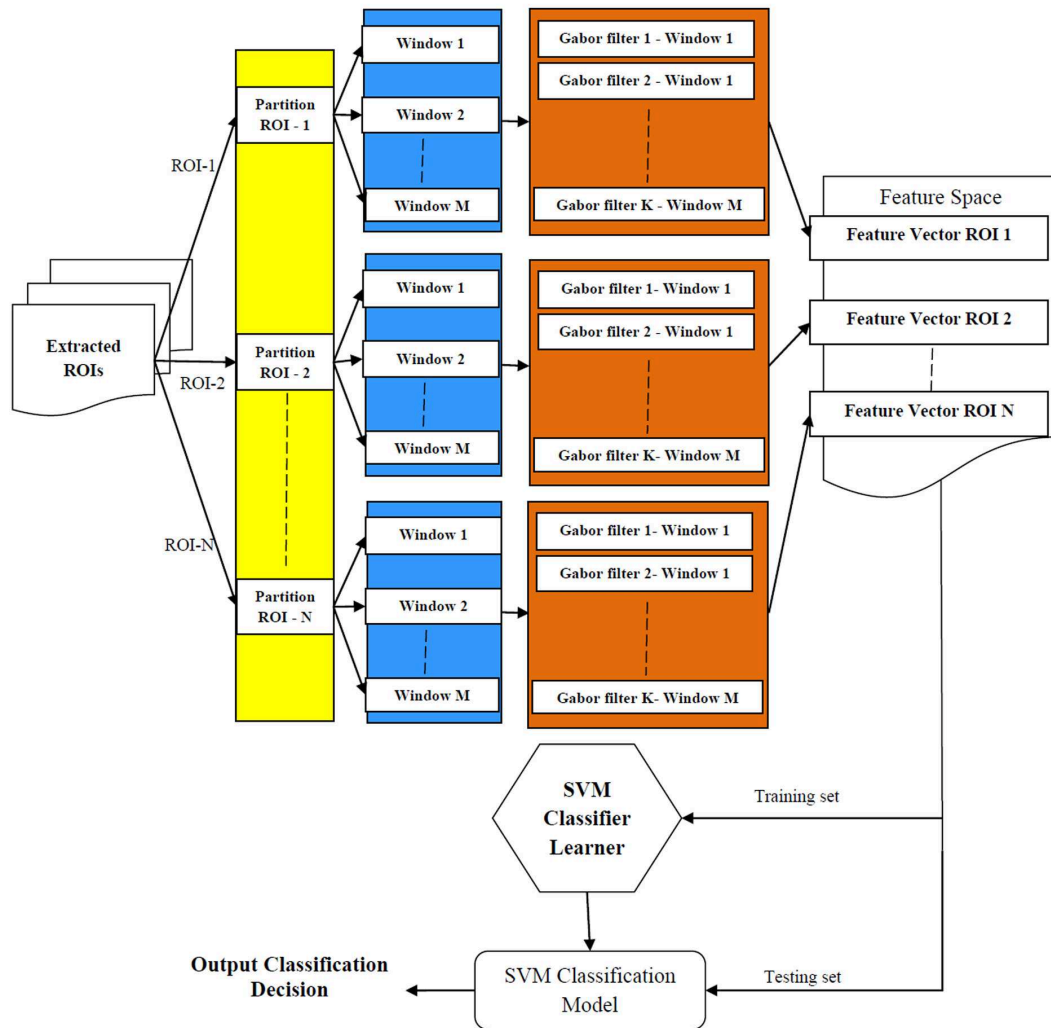
Figure 1 Block diagram of the proposed method. Here N = total number of ROIs in the database, M = total number of windows in an ROI and K = total number of filters in a Gabor bank.

description of the proposed method is shown in Figure 1. In the following subsections, we elaborate the method.

3.1.1. Gabor filters

In this section, we give a brief overview of the Gabor filters. Gabor filters are biologically motivated convolution kernels and their response is found to be similar to receptive fields of neurons in the visual cortex [7]. An interesting property of these filters is that they possess optimal joint localization both in frequency and spatial domains [7]. They have enjoyed wide usage in a myriad of applications in the fields of computer vision and image processing e.g. face recognition [9], vehicle detection [8] and texture analysis [10] etc. A two-dimensional Gabor filter defined as a Gaussian kernel modulated by an oriented complex

sinusoidal wave can be described as follows [8]:

$$g(x,y) = \frac{1}{2\pi\sigma_x\sigma_y} e^{\left[-\frac{1}{2}\left(\frac{\tilde{x}^2}{\sigma_{\tilde{x}}^2} + \frac{\tilde{y}^2}{\sigma_{\tilde{y}}^2}\right)\right]} e^{(2\pi j W \tilde{x})} \quad (1)$$

$$\tilde{x} = x.cos\theta + y.sin\theta \ \ and \ \ \tilde{y} = x.sin\theta + y.cos\theta \quad (2)$$

where σ_x and σ_y are the scaling parameters of the filter and describe the neighborhood of a pixel where weighted summation takes place, W is the central frequency of the complex sinusoidal wave and is the orientatio n of the normal to the parallel stripes of the Gabor function and is termed as the orientation of a Gabor filter. A filter will have stronger response to an edge where the normal is parallel to the orientation In order to extract textural micro-patterns in mammogram ROIs, Gabor filters can be tuned with different orientations and scales, and thus provide a powerful

tool for the description of textural properties of masses at different scales and orientations.

Gabor filter bank

A Gabor filter bank contains multiple Gabor filters tuned with different parameter settings (scaling, orientation and central frequency). In this paper, we investigate the effect of Gabor filter banks with different scale and orientation settings such as Gabor filter bank containing 6 filters (referred to as GS2O3: 2 scalesS × 3 orientationsO), 15 filters (GS3O5), 24 filters (GS4O6) and 40 filters (GS5O8). In each case the initial maximum frequency is equal to 0.2 and the initial orientation is set to 0. The orientations and frequency for a bank are calculated using following equations [8]:

$$orientation(i) = \frac{(i-1)\pi}{O}, \ i = 1, 2, ..., O \quad (3)$$

$$frequency(i) = \frac{f_{\max} = 0.2}{(\sqrt{2})^{i-1}}, \ i = 1, 2, ..., S \quad (4)$$

where O is the total number of orientations and S is that of scales. For instance, the bank GS5O8 has, for five scales, the frequencies (0.2, 0.14, 0.1, 0.07 and 0.05) and the orientations (0, 22.5, 45, 67, 90, 112.5, 135 and 157 in degrees). In Figures 2 and 3, two filters from this bank with (f = 0.2, O = 0°) and (f = 0.05, O = 157.5^o) are shown for an image of size 256×256. Figure 4 shows the combined frequency response of all 40 filters in this bank.

Figure 2 Gabor Filter with frequency = 0.2, orientation = 0 degree.

Figure 3 Gabor Filter with frequency = 0.05, orientation = 157.5 degree.
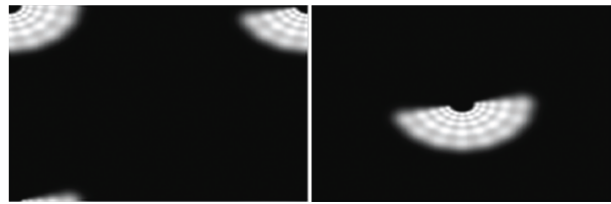

Figure 4 Combined frequency response of the 40 filters in the Gabor bank

3.1.2. Partitioning of ROIs

One common approach to extract features using Gabor filter bank is to filter an ROI with Gabor filters, calculate the statistical measures like mean, standard deviation, skewness etc. from magnitudes of the filter responses. But the features extracted in this way does not keep the spatial locality of texture micropatterns. To extract statistical features of texture micropatterns existing with different scales and orientations at different locations, we partition each ROI into overlapping windows. This approach takes into account the spatial locality of micropatterns, and the extracted features are more discriminative. First each ROI is partitioned into blocks and then using these blocks, overlapping windows are defined. To be precise, an ROI, say, of size 512×512 is first divided into blocks of equal sizes e.g. 128×128 pixels, as is depicted with squares enclosed with black lines in Figure 5. In this way, sixteen blocks are created, which are labeled 1-16 in Figure 5. The blocks are then combined to create overlapping windows e.g. blocks 1, 2, 5 and 6 form the first window of size 256×256, blocks 2, 3, 6 and 7 the second, blocks 5, 6, 9 and 10 the fourth, and so on. With this formation, 9 overlapping windows are created. First window is visualized with transparent red color rectangle in Figure 5. It may please be noted that by increasing/ decreasing the size of a block, ROI can be partitioned into different numbers of windows of different sizes.
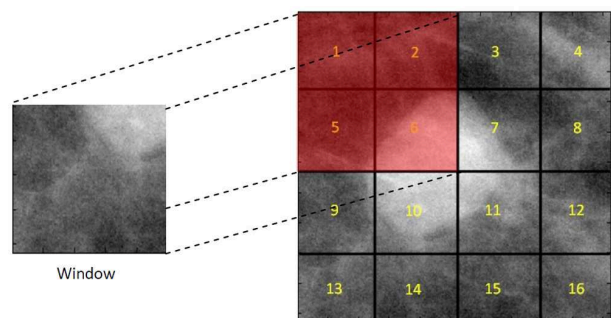

Figure 5 Segmentation of ROI in patches and sub-windows

3.1.3. Feature Extraction

Our approach for feature extraction using Gabor filter bank is similar to the design strategy that has been used for texture based feature extraction for vehicle detection [8] and image retrieval [10]. For extracting features each window is convolved with a Gabor filter bank. The raw responses of Gabor filter bank can be used as features for classification but this representation suffers from two problems: first, the dimension of the feature space becomes prohibitively high; second there is a lot of redundancy. It is necessary to perform some processing to acquire the most representative features which does not suffer from the above mentioned problems; examples of such features are Gabor energy and moments of Gabor filter bank responses [8, 11]. Similar to the approach given in [8] for vehicle detection, in this paper, the magnitude response of each Gabor filter in the bank is computed from each window of an ROIs and is represented by three statistical measures: the mean , the standard deviation and the skewness (where i corresponds to the ith filter in the bank and j to the jth window). These features correspond to the statistical properties of a group of pixels in a window; in this way, the location of pixels is not taken into account. This strategy compensates for any errors that might occur during petitioning of ROIs into windows. As an example of our approach for feature extraction, consider the Gabor filter bank of 40 filters (5 S × 8 O). Applying this bank on 9 windows (see Figure 5) of an ROI, yields a feature vector of length 1080 [= 40(filters)×9(windows)3(moments)], as shown in the following :$[u_{1,1}, \sigma_{1,1}, k_{1,1}, u_{2,1}, \sigma_{2,1}, k_{2,1}, u_{40,1}, \sigma_{40,1}, k_{40,1}, u_{1,2}, \sigma_{1,2}, k_{1,2}, ...u_{40,9}, \sigma_{40,9}, k_{40,9}]$. For each ROI, we compute this feature vector that represents the ROI. The dimension of the feature space depends on the number of overlapping windows and the number of filters in a Gabor filter bank. We investigated the impact of the sizes of ROIs, the number of overlapping windows, and the number of filters. The effect of these parameters has been presented and discussed in detail Section 4.

3.2. Support Vector Machines (SVM)

False positive reduction and the discrimination between benign and malignant masses are both classification problems. A classification problem encompasses the assignment of an unknown pattern to a predefined class, according to the characteristics of the pattern, presented in the form of a feature vector. Numerous classification techniques exist. We used SVM for the classification of ROIs. In our case, we are dealing with a binary classification problem, where an ROI is to be classified either cancer region or normal. SVM classifiers [12] are the most advanced ones, generally, designed to solve binary classification problems; thus perfectly suite our requirements. SVM finds an optimal hyper-plane that separates the data belonging to different classes with large margins in a high dimensional space [13]. The margin is defined as the sum of distances to the decision boundary (hyper-plane) from the nearest points (support vectors) of the two classes. SVM formulation is based on statistical learning theory and has attractive generalization capabilities in linear as well as non-linear decision problems [12, 14]. SVM uses structural risk minimization as opposed to empirical risk minimization [12] by reducing the probability of misclassifying an unknown pattern drawn randomly from a fixed but unknown distribution. Let be a training set where is the feature vector of ith training pattern containing J features, is the class label of having the value +1 or -1 depending its class. Finding an optimal hyper-plane with maximum margin implies solving a constrained optimization problem using quadratic programming and can be stated as:

$$f(x) = \sum_{i=1}^{N} \alpha_i y_i k(x_i, x) + b \qquad (5)$$

where α_i are the Lagrange multipliers, $k(x_i, x)$ is the kernel function and sign of $f(x)$ gives the membership class of x. For linearly separable problems, kernel function is simply the dot product of the two given points in the input space. However, for the problems, which are not linearly separable, the original input space is mapped to a higher dimensional space, possibly making the data linearly separable, using a kernel function that satisfies the Mercer's condition [12]. In this new formulation, the misclassification penalty or error is controlled with a user defined parameter C known as regularization parameter that controls the trade-off between error of SVM and margin maximization, and is tied to the kernel. There exist several kernels e.g. linear, polynomial, sigmoid, radial basis function (RBF) etc. In our experiments, RBF kernel is used as given by:

$$k(x_i, x) = \exp(-\gamma||x_i - x||^2), \gamma > 0 \qquad (6)$$

where γ is the width of the kernel function. There are two parameters now tied to RBF kernel: and C. Tuning these parameters in an attempt to find a better hypothesis is called model selection procedure. For model selection, we first perform a loose grid search (coarse search for computational efficiency) in the parameter space to find the potential region containing optimal parameter values. Later, the fine grid search is conducted in this region to find the optimal parameters. This model selection procedure is recommended in the work of Chih-Wei Hsu et. al. [15]. The selected parameters are fed into the kernel and SVM is finally applied to our data sets. Detailed discussion on the statistical formulation and computational aspects of SVM can be found in the work of Vapnik [12].

4. Results and Discussion

In this section, we present the results of the proposed method and discuss them. We conducted the experiments for two problems: false positive reduction i.e. to classify ROIs into

normal and mass and, the classification of mass ROIs into benign and malignant. For the first problem, we explore two different aspects: (i) discrimination between suspicious normal ROIs and cancer (malignant mass) ROIs, and (ii) discrimination between suspicious normal ROIs and true mass (benign and malignant). First, we give the overview of the database that is used for the validation of the proposed method. Then we discuss the results for each problem. The extracted ROIs are in different sizes, for processing them with Gabor filter bank, it is necessary to resize them into the same resolution; we tested four different resolutions: 512×512, 256×256, 128×128 and 64×64. We statistically compare the effect of different ROI resolutions using a non-parametric Friedman test with Holm post-hoc test [35, 36]. For extracting features, each ROI can be partitioned into blocks of different sizes for defining overlapping windows. We tested five block sizes: 128×128, 64×64, 32×32, 16×16 and 8×8. Finally, the proposed method is compared with state-of-the art methods.

4.1. Database and Evaluation Methodology

The proposed method is evaluated using Digital Database for Screening Mammography (DDSM) [32]; this database consists of more than 2000 cases and is commonly used as a benchmark for testing new proposals dealing with processing and analysis of mammograms for breast cancer detection. Each case in this database is annotated by expert radiologists; the complete information is provided as an overlay file. The locations of masses in mammograms specified by experts are encoded as code-chains. We randomly selected 1024 (512 normal but suspicious, 256 malign and 256 benign) cases from the database. Using code chains, we extracted 256 ROIs which contain true masses; the rolutions of these ROIs vary depending on the sizes of the mass regions. In addition, we extracted 512 ROIs containing normal but suspicious tissues and 256 benign ROIs. Some sample ROIs are shown in Figure 6. The evaluation of the method is performed using tenfold cross validation. In particular, a data set is randomly partitioned into ten non-overlapping and mutually exclusive subsets. For the experiment of fold i, subset i is selected as testing set and the remaining nine subsets are used to train the classifier. Using tenfold cross validation, the performance of the method can be confirmed against any kind of bias involved in the selection of the samples for training and testing phases. It also helps in determining the robustness of the method when tested over different ratios of normal and abnormal ROIs used as training and testing sets (due to random selection, ratios will be different). The SVM classifier gives a membership value of each class when an unknown pattern is presented to it. The ROC (receiver operator characteristics) curve can be obtained by varying the threshold on this membership value. The area under ROC curve (Az) is used as a performance measure. The other commonly used evaluation measures are accuracy or recognition rate $(RR) = (TP+TN)/(TP+FP+TN+$

$FN)$, sensitivity $(Sn) = TP/(TP + FN)$, specificity $(Sp) = TN/(TN+FP)$, where TN is the number of true negatives, TP is that of true positives, FP is that of false positives and FN denotes the number of false negatives. To validate the performance of the proposed method and compare with stat-of-the-art methods, we employ these performance measures. We performed experiments with four different resolutions: 512×512, 256×256, 128×128, and 64×64. All ROIs are scaled to one of these resolutions. The effect of each resolution on the classification accuracy is analyzed to know which resolution results in the best performance. In order to extract features at different level of granularities, we partition the ROIs into overlapping windows of different sizes. The overlapping windows make it possible to analyze those textural micropatterns of masses that might be present at the boundaries of the windows. The windows sizes are dependent on block sizes as discussed in Section 3.1.1. We tested the performance of the proposed method over five different patch sizes (128×128, 64×64, 32×32, 16×16 and 8×8 pixels). The Gabor filter banks with four configurations of scales and orientations are used: GS2O3, GS3O5, GS4O6 and GS5O8. Gabor filter banks with different settings can extract local textural features at different scales and orientations. Each Gabor filter bank is initialized with initial max frequency = 0.2, initial orientation = 0 degree and applied to each window corresponding an ROI; three statistical measures (mean, standard deviation and skewness) are calculated from the magnitude of each Gabor filter response and concatenated to form a feature vector.
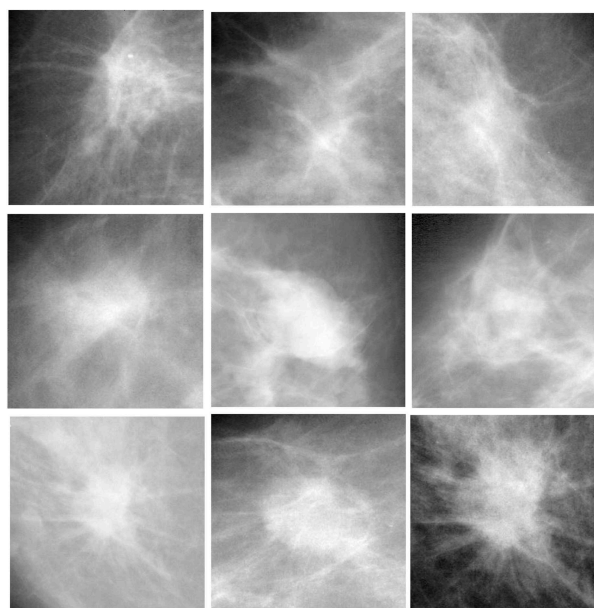

Figure 6 (Top row) normal but suspicious ROIs, (middle row) benign mass ROIs, (bottom row) malignant mass ROIs

4.2. Experimental Results for Suspicious Normal and Cancer ROIs

In this subsection, we give the results of the discrimination between normal but suspicious ROIs and cancer (malignant mass) ROIs. For different choices of ROI resolutions, window sizes, and Gabor filter banks, the performance results are given in Table 1.

Figure 7(a) shows the impact of block sizes on the recognition accuracy in terms of area under ROC curve. The best result (Az = 0.99±0.02) is obtained with block size 8×8; it is due to the reason that small block sizes allow to capture the spatial locality of micro-patterns in a better way. The extracted features from each window (consisting of 4 blocks) are statistical measures (mean, standard deviation, skewnes), which are global; when they are extracted with smaller block sizes, they keep the spatial locality as well; in this way the extracted features become a blend of local and global features. The best accuracy (99.02±1.39), the best specificity (99.63±1.17), and the best sensitivity (99.63±1.17) are also obtained with block size 8 × 8, see Table 1.

Figure 7(b) depicts the effect of different configurations of Gabor filter bank. The best value of Az is obtained with GS5O8 (5 scales and 8 orientations); it is due to the reason that the micro-patterns at different scales and orientations are represented in a better way. From Table 1, it is obvious that the best accuracy (99.02±1.39), the best specificity (99.63±1.17), and the best sensitivity (99.63± 1.17) are also obtained with GS5O8.

The effect of resolution is shown in Figure 7(c). The overall best accuracy (Az = 0.99±0.02) in terms of area under ROC curve is obtained with resolution 128×128. When the resolution is increased or decreased, the Az values decreases. It is due to the reason that in case of low resolution the necessary discriminatory information is lost whereas high resolution results in copious of redundant features.

4.3. Experimental Results for Suspicious Normal and Mass ROIs

In this section, we present the performance results for the discrimination of normal but suspicious and mass (benign and malignant) ROIs. This aspect of the false negative problem is relatively more difficult than the one discussed in Section 4.2. Some of the benign cases are difficult to discriminate from suspicious normal ROIs; although, most of the benign masses are structurally more closer to the malignant masses, there are benign masses however, that are structurally closer to normal tissues; it makes discrimination task difficult. It is therefore expected a decline in the recognition rate as depicted in Table 2, as compared to the results presented in Table 1. In this case, the best result in terms of Az value is observed for ROI resolution of 512×512 pixels with block size of 64×64 and Gabor filter bank GS3O5.

In Figure 8 (a, b, c), the best average Az values and other performance measures are plotted for different block sizes, four Gabor filter banks and four ROI resolutions used in the experiments. According to Figure 8 (a), the best ROI resolution is 512×512 with block size 64×64 and Gabor filter bank GS3O5 (in terms of Az value). Figure 8(b) shows that the Gabor filter bank GS3O5 gives the best Az value as compared to other configurations for ROI resolution of 512×512. In the same way, comparing the ROI resolutions in Figure 8 (c), it is observed that ROI resolution of 512×512 pixels results the best performance in terms of accuracy, Az value and specificity. It is observed that low resolutions 128×128 and 256×256 are not very much effective for this case (both in terms of accuracy and Az. value), see Figure 8(c) and Table 2.It is interesting to note that the results obtained with resolution 64×64 are close to those obtained with resolution 512×512. In case of 64×64 resolution, the best Az value of 0.95±0.03 and average percentage accuracy of 94.33% are obtained with block size 8×8 and Gabor filter bank GS5O8; the total number of features is 7840. However, resolution 512×512 yield the best Az value of 0.96±0.02 and average percentage accuracy of 94.53±2.73 when block size 64×64 and Gabor filter bank GS3O5 is used; the total number of features is 2940. The drop of performance in case of 64×64 resolution is due to the reason that in this case there are a large number of redundant features. Once the redundancy is removed using feature selection, this resolution of ROIs may perform better.

4.4. Experimental Results for Benign and Malignant ROIs

This section summarizes the results for the most difficult classification problem i.e. the discrimination between benign and malignant.This discrimination task is hard in this case due to highly identical patterns and similar structures of two classes (benign and malignant) of digital mammograms. The results are shown in Table 3; both the best average accuracy and Az value are obtained (see Table 3) for ROI resolution of 128×128 with block size of 8×8 when filtered with GS5O8. After analyzing the plots in Figure 9 (a, b and c), the best block size is 8×8 pixels, and the best Gabor filter bank is GS5O8 with ROI resolution of 128×128 (in terms of Az value). Also, the best ROI resolution is 128×128 pixels (in terms of Az value and accuracy). However for sensitivity, the best performance is obtained with ROI resolution of 512×512.

4.5. Discussion based on Statistical Significance

To test whether a specific ROI resolution performs significantly better than the others, a non-parametric statistical test (Friedman) is employed. The Friedman test is chosen because it does not make any assumptions about the distribution of the underlying data; it is a recommended and

Table 1 Mean performance measures based on varying window sizes, different configurations of Gabor filter banks and ROI resolutions using tenfold cross validation.

Res.	Block Size	Gabor bank	Sn	Sp	Acc.(%)	Az.
64×64	16×16	GS2O3	95.57	97.18	96.47	0.96±0.03
		GS3O5	96.68	98.58	97.45	0.97±0.02
		GS5O8	97.34	99.26	98.43	0.98±0.02
	8×8	GS2O3	96.25	96.81	96.67	0.97±0.02
		GS3O5	97.93	98.57	98.04	0.98±0.03
		GS4O6	97.60	98.47	98.04	0.98±0.04
		GS5O8	98.39	**99.63**	**99.02**	0.98±0.02
128×128	32×32	GS2O3	95.05	97.47	96.27	0.97±0.03
		GS3O5	95.98	96.32	96.27	0.96±0.03
		GS4O6	97.22	98.04	97.65	0.97±0.01
		GS5O8	97.67	99.18	98.43	0.98±0.03
	16×16	GS2O3	96.47	97.45	97.06	0.96±0.03
		GS3O5	96.53	98.85	97.65	0.98±0.02
		GS4O6	97.08	98.80	97.84	0.98±0.02
		GS5O8	97.02	98.40	97.65	0.97±0.04
	8×8	GS2O3	95.77	96.64	96.27	0.97±0.03
		GS3O5	97.31	98.43	97.84	0.97±0.03
		GS4O6	95.80	96.86	96.47	0.97±0.02
		GS5O8	**98.90**	98.82	98.82	**0.99±0.02**
256×256	64×64	GS2O3	96.48	96.66	96.47	0.96±0.03
		GS3O5	96.99	97.01	96.86	0.97±0.02
		GS4O6	97.70	97.51	97.65	0.98±0.02
		GS5O8	97.69	98.29	98.04	0.97±0.03
	3232	GS2O3	97.05	97.73	97.25	0.98±0.01
		GS3O5	97.59	97.29	97.45	0.97±0.03
		GS4O6	97.55	98.83	98.24	0.98±0.02
		GS5O8	96.79	98.46	97.65	0.97±0.02
	16×16	GS2O3	95.20	97.60	96.47	0.97±0.03
		GS3O5	96.82	97.95	97.45	0.97±0.03
		GS4O6	96.81	98.09	97.25	0.98±0.03
		GS5O8	95.90	97.83	96.86	0.96±0.02
512×512	128×128	GS2O3	96.43	95.10	95.49	0.96±0.05
		GS3O5	97.63	94.61	96.07	0.95±0.03
		GS4O6	97.23	96.89	96.86	0.97±0.03
		GS5O8	97.19	97.99	97.64	0.97±0.03
	64×64	GS2O3	97.18	97.63	97.25	0.97±0.03
		GS3O5	97.29	98.56	97.84	0.98±0.02
		GS4O6	97.95	98.00	98.04	0.98±0.02
		GS5O8	98.05	98.06	98.04	0.98±0.02
	32×32	GS2O3	96.20	95.86	96.08	0.96±0.04
		GS3O5	97.34	98.05	97.65	0.98±0.02
		GS4O6	97.25	97.68	97.45	0.97±0.03
		GS5O8	96.67	97.22	97.06	0.97±0.02

suitable test for comparing a set of classification strategies over multiple performance output values. For comparison, we selected the eight best mean accuracy and mean Az values for different ROI resolutions according to the guidelines presented in [35,36]. Best eight values are selected because for ROI resolution of 64×64 only eight experimental outputs are available. Table 4 presents the summary of the comparisons of the best ROI resolution (the resolution with the best average rank, considered as control resolution) with the remaining ROI resolutions accord-

ing to the non-parametric Friedman test with the Holm's post-hoc test [35,36] in terms of percentage accuracy and Az values as given in Table 1-3. For each ROI resolution, the average rank (the lower the average rank the better the algorithm's performance), the p-value (when the average rank is compared to the average rank of the ROI resolution with the best rank i.e. control resolution) and Holm critical value obtained by Holm's post-hoc test are reported. Based on the fact that the p-value is lower than the critical value (at 5% significance level), its value is shown in
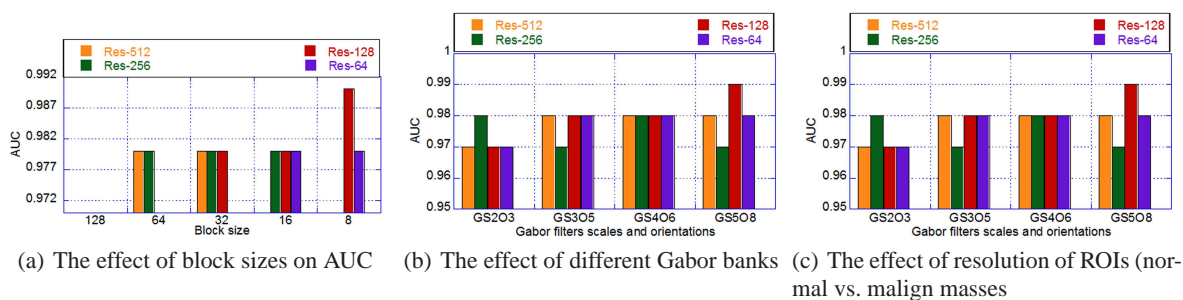
(a) The effect of block sizes on AUC (b) The effect of different Gabor banks (c) The effect of resolution of ROIs (normal vs. malign masses

Figure 7 The effects of different parameters on the classification accuracy for the case normal tissue vs. malignant masses.

(a) The effect of block sizes on AUC (b) The effect of different Gabor banks (c) The effect of resolution of ROIs (normal vs. malign masses
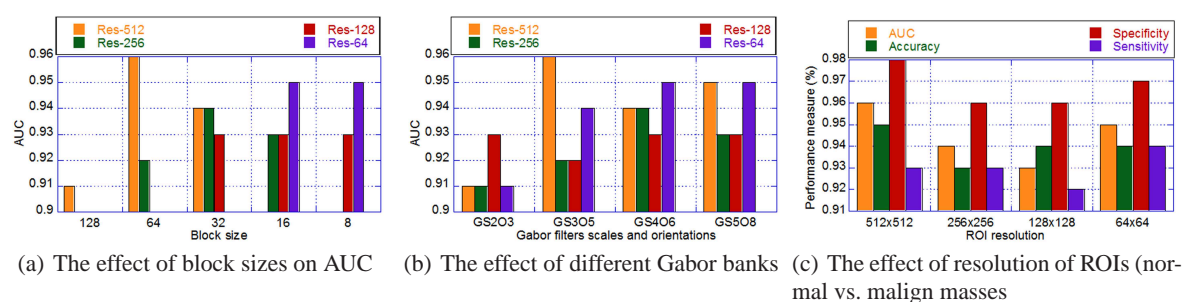
Figure 8 The effects of different parameters on the classification accuracy for the case normal tissues vs. masses.

(a) The effect of block sizes on AUC (b) The effect of different Gabor banks (c) The effect of resolution of ROIs (normal vs. malign masses
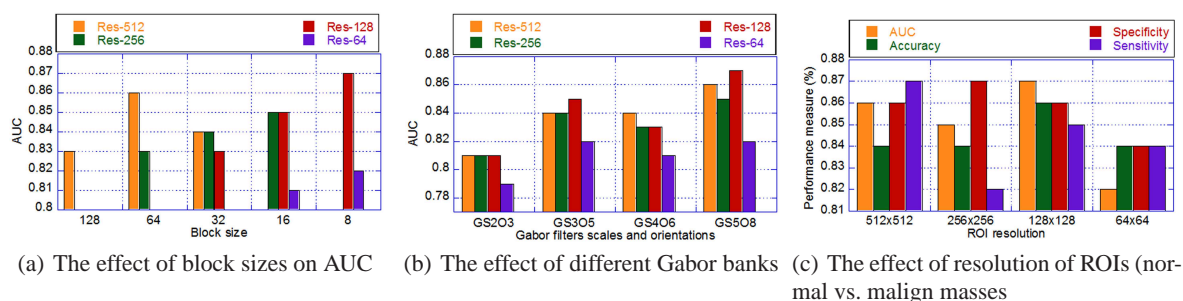
Figure 9 The effects of different parameters on the classification accuracy for the case normal tissues vs. masses.

bold when there is a significant difference between the average ranks of an ROI resolution and the control ROI resolution, and it shows that the control ROI resolution has significantly outperformed the corresponding ROI resolution. According to the statistics of Table 4, ROI resolution of 128×128 is the best performing resolution for the problem of discrimination between normal and cancer ROIs in terms of eight best mean percentage accuracy values with an average rank of 1.6875, followed by ROI resolutions 512×512, 256×256 and 64×64. However, the difference between the performances of the four resolutions is not statistically significant. For the other statistical tests, reso-

lution of 512×512 is selected as control configuration because its performance is better than resolutions; at least in terms of best eight performance values of accuracy as well as Az. There are only three cases (bold values) where the differences between control resolution and the resolutions 256×256 and 64×64 are statistically significant in terms of average accuracy and Az value. This leads to the conclusion that all ROI resolutions (used in the experiments) can safely be used with the proposed method for the classification problems (normal vs. malignant masses) and (normal vs. masses) i.e. for false positive reduction problem. For the classification problem (benign vs. ma-

Table 2 Performance evaluation based on varying sub-window sizes, configuration of Gabor banks and different ROI resolutions using tenfold cross validation (normal vs. masses)

Res.	Block Size	Gabor bank	Sn	Sp	Acc.(%)	Az.
64×64	16×16	GS2O3	89.42	92.12	90.82	0.91±0.05
		GS3O5	88.04	93.51	90.44	0.91±0.05
		GS4O6	90.99	94.80	92.76	0.92±0.04
		GS5O8	**93.97**	94.81	94.33	0.95±0.03
	8×8	GS2O3	87.90	94.35	90.84	0.90±0.04
		GS3O5	91.95	96.95	94.33	0.94±0.03
		GS4O6	91.85	96.04	93.94	0.95±0.04
		GS5O8	92.66	95.85	94.13	0.95±0.03
128×128	32×32	GS2O3	89.75	93.68	91.41	0.91±0.05
		GS3O5	91.01	92.34	91.40	0.92±0.03
		GS4O6	91.82	93.45	92.59	0.93±0.04
		GS5O8	92.13	93.16	92.58	0.92±0.05
	16×16	GS2O3	91.28	96.19	93.74	0.93±0.04
		GS3O5	88.50	94.12	91.20	0.90±0.04
		GS4O6	90.72	92.64	91.59	0.91±0.06
		GS5O8	90.46	95.27	92.76	0.93±0.04
	8×8	GS2O3	87.10	93.60	90.25	0.92±0.06
		GS3O5	87.26	94.47	90.83	0.91±0.04
		GS4O6	88.47	94.21	91.40	0.89±0.05
		GS5O8	91.67	93.56	92.57	0.93±0.05
256×256	64×64	GS2O3	88.06	92.88	90.26	0.90±0.07
		GS3O5	87.61	93.88	90.83	0.92±0.05
		GS4O6	92.28	93.44	92.78	0.91±0.03
		GS5O8	92.14	91.88	92.00	0.92±0.05
	32×32	GS2O3	88.05	95.33	91.79	0.91±0.03
		GS3O5	89.21	95.06	91.79	0.92±0.05
		GS4O6	90.61	94.99	92.77	0.94±0.04
		GS5O8	92.60	93.81	93.17	0.93±0.04
	16×16	GS2O3	85.45	92.69	89.07	0.89±0.03
		GS3O5	89.18	95.81	92.39	0.92±0.04
		GS4O6	89.20	95.94	92.36	0.92±0.05
		GS5O8	90.20	95.18	92.56	0.93±0.04
512×512	128×128	GS2O3	88.43	92.79	90.41	0.91±0.05
		GS3O5	90.39	91.39	91.04	0.91±0.04
		GS4O6	89.12	92.42	90.83	0.91±0.05
		GS5O8	89.43	92.51	91.00	0.90±0.04
	64×64	GS2O3	90.76	92.60	91.21	0.91±0.04
		GS3O5	91.14	**97.67**	94.53	**0.96±0.02**
		GS4O6	93.42	96.49	**94.92**	0.94±0.04
		GS5O8	92.97	95.33	93.96	0.95±0.04
	32×32	GS2O3	84.73	93.96	89.46	0.89±0.05
		GS3O5	88.35	96.25	91.98	0.93±0.06
		GS4O6	89.40	96.10	92.77	0.94±0.04
		GS5O8	88.97	96.53	92.77	0.936±0.06

lignant), however, low resolutions of ROIs can make the performance worse e.g. as observed for 6464 resolution.

4.6. Comparison with other methods

It is a hard task to critically compare our work with various methods present in the literature in detail for the target problems, mainly because of following reasons:

–The mammogram database used to evaluate the methods is different.
–Given that the same database is used, the sample mammograms selected for experiments are not necessarily same.
–Total number of mammograms used in different research works is not same.
–A different experimental setup is used e.g. k-fold validation with varying k value, training and testing set

Table 3 Performance evaluation based on varying sub-window sizes, configuration of Gabor banks and different ROI resolutions using tenfold cross validation (benign vs. malign)

Res.	Patch Size	Gabor Bank	Sn	Sp	Acc.%	Az.
64×64	16×16	GS2O3	78.20	77.34	77.76	0.78±0.07
		GS3O5	79.29	76.94	78.11	0.79±0.06
		GS4O6	80.78	79.29	80.07	0.81±0.05
		GS5O8	81.97	78.08	80.08	0.81±0.07
	8×8	GS2O3	78.89	78.20	78.52	0.79±0.07
		GS3O5	79.58	82.86	81.23	0.82±0.07
		GS4O6	80.08	81.74	80.83	0.80±0.07
		GS5O8	83.54	83.97	83.77	0.82±0.06
128×128	32×32	GS2O3	79.25	80.06	79.68	0.79±0.04
		GS3O5	81.11	80.86	81.04	0.81±0.06
		GS4O6	80.49	81.69	81.05	0.83±0.04
		GS5O8	80.03	83.15	81.63	0.81±0.07
	16×16	GS2O3	80.42	79.28	79.87	0.81±0.06
		GS3O5	84.40	82.02	83.21	0.85±0.05
		GS4O6	81.20	82.00	81.64	0.83±0.06
		GS5O8	81.18	82.37	81.83	0.82±0.08
	8×8	GS2O3	76.60	81.98	79.30	0.79±0.06
		GS3O5	78.52	82.88	80.67	0.81±0.05
		GS4O6	79.77	83.97	81.86	0.79±0.06
		GS5O8	85.09	85.97	**85.53**	**0.87±0.05**
256×256	64×64	GS2O3	79.37	79.23	79.31	0.78±0.05
		GS3O5	80.08	80.95	80.49	0.81±0.05
		GS4O6	78.54	80.88	79.70	0.77±0.08
		GS5O8	79.66	83.92	81.81	0.83±0.05
	32×32	GS2O3	81.25	81.28	81.24	0.81±0.07
		GS3O5	79.98	86.35	83.18	0.84±0.05
		GS4O6	82.43	82.85	82.61	0.83±0.04
		GS5O8	80.77	85.55	83.20	0.82±0.07
	16×16	GS2O3	78.18	80.08	79.12	0.79±0.07
		GS3O5	76.94	83.65	80.26	0.82±0.06
		GS4O6	76.54	85.20	80.87	0.82±0.05
		GS5O8	81.58	**87.11**	84.37	0.85±0.03
512×512	128×128	GS2O3	78.20	76.92	77.55	0.78±0.09
		GS3O5	80.88	79.29	80.07	0.81±0.06
		GS4O6	79.34	80.86	80.09	0.80±0.03
		GS5O8	81.62	82.03	81.84	0.83±0.05
	64×64	GS2O3	86.29	79.26	82.82	0.81±0.06
		GS3O5	83.62	85.18	84.38	0.84±0.09
		GS4O6	87.12	81.60	84.39	0.83±0.05
		GS5O8	84.34	84.03	84.19	0.86±0.05
	32×32	GS2O3	**87.49**	76.18	81.84	0.81±0.06
		GS3O5	83.92	84.02	83.97	0.84±0.04
		GS4O6	82.82	83.66	83.19	0.84±0.05
		GS5O8	80.45	85.58	83.01	0.81±0.05

formation with different percentages of ROIs, evaluation on a validation set etc.

– Ratios of ROIs for different classes e.g. normal, malignant and benign are not same for all the methods.

However, our aim is to have general trends of performance comparison and we compare our method with other techniques on the basis of accuracy and Az values. The quantities that are not reported in the respected research works are indicated with dash symbol in Table 5. For some methods, standard deviation values are not available. The quantities are average values followed by standard deviations. For the two problems, only the best results are extracted for all the methods being compared. The proposed method gives comparable performance as compared to the results published in the recent literature. The Az value is greater than the majority of the methods in comparison and the percentage accuracies are also acceptable and encourag-

Table 4 Summary of the comparisons of different ROI resolutions for eight best performance output values (i.e. in terms of (i) eight best Az. values and (ii) eight best percentage accuracy values) according to the non-parametric Friedman test with the Holm's post-hoc test

Comparision on the basis	Experiment case	Res.	Avg.rank	p	Holm
Accuracy	Normal vs. Malignant	128×128(control)	1.6875	-	-
		512×512	2.875	0.0658	0.025
		256×256	2.9375	0.0528	0.017
		64×64	2.5	0.208	0.05
	Normal vs. Masses	512×512 (control)	1.875	-	-
		256×256	2.625	0.24528	0.025
		128×128	3.0	0.0813	0.017
		64×64	2.5	0.3329	0.05
	Benign vs. Malignant	512×512 (control)	1.125	-	-
		256×256	2.625	0.02014	0.025
		128×128	2.25	0.0814	0.05
		64×64	4.0	$8.431227E^{-6}$	0.017
Az. value	Normal vs.Malignant	512×512 (control)	1.875	-	-
		256×256	2.75	0.175	0.025
		128×128	2.4375	0.384	0.05
		64×64	2.9375	0.0998	0.017
	Normal vs.Masses	512×512 (control)	1.75	-	-
		256×256	2.75	0.121	0.025
		128×128	2.9375	0.0658	0.017
		64×64	2.5625	0.20813	0.05
		512×512 (control)	1.625	-	-
		256×256	2.25	0.3329	0.025
		128×128	2.125	0.43858	0.05
		64×64	4.0	$2.3384368E^{-4}$	0.017

Table 5 Comparison with state-of-the-art methods based on Acc. and Az values

problem	research work	database	No. of ROIs	Acc. (%)	Az
Normal vs. Masses	Fatemeh et. al. [34](2010)	MIAS	90	85.9±0.03	-
	Daniel et. al. [30] (2011)	DDSM	5090	90.07	-
	Ioan B. et. al. [16](2011)	MIAS	322	84.37	0.79
	X. Liado et. al. [3](2009)	DDSM	512	-	0.94±0.02
	Our Method	DDSM	512	**94.92±2.30**	**0.96±0.02**
Benign vs. Malignant	Fatemeh et. al. [34] (2010)	MIAS	90	87.00±0.008	-
	Daniel et. al. [30] (2011)	DDSM	3240	84.22	-
	Ioan B. et. al. [16] (2011)	MIAS	114	78.26	0.78
	Our Method	DDSM	512	**85.53±5.43**	**0.87±0.05**

ing. This indicates that the proposed method has the potential to be further investigated.

5. Conclusion

In this article, we addressed two problems: false positive reduction i.e. discrimination between normal but suspicious and mass ROIs, and the classification of benign and malignant mass ROIs. A novel technique is presented for extracting local directional spatial textural features from digital mammograms using different configurations of Gabor filter bank and different resolutions of ROIs. These features best discriminate between the three tissue types

(normal, benign and malign masses) and in general, improve the recognition rate of a breast cancer detection system. The method is evaluated over 1024 ROI images using Support Vector Machine. The results for low resolution ROIs are encouraging as the feature space become more compact and the recognition rate of cancerous tissues in the digital mammograms has improved. Model compactness indirectly implies that the feature space will be low dimensional and thus better computational efficiency and better generalization of the classification model is expected and observed. Among different configurations of Gabor filter bank, the one with 5 scales and 8 orientations gives over all best results, because it captures the texture micropatterns present in mammograms at different scales

and orientations in a better way.The experimental results are compared with the results presented in some best recent research works. We observed that the performance of our approach is up to the mark and its performance is comparable.

There are several future avenues in order to extend the proposed technique. The recognition accuracy is affected by the dimension of the feature space. With different configurations of Gabor filter bank, different resolutions of ROIs and different block sizes, feature space of different dimensions are obtained, which may include a lot of redundant features. Therefore it is necessary to explore feature selection techniques to get rid of redundancy from the feature spaces. Another issue is to find the optimal Gabor filter bank for better description of texture properties. We plan to investigate evolutionary computation techniques for the optimization of Gabor filter bank. It will also be interesting to investigate the performance of the proposed method on other complex problems like detection of micro-calcification, breast structural disorders etc.

Acknowledgement

References

[1] SF. Altekruse, CL. Kosary, M. Krapcho, et al, SEER Cancer Statistics Review, Bethesda, MD: National Cancer Institute, 1975-2007 (2010).

[2] Z. Yufeng, "Breast Cancer Detection with Gabor Features from Digital Mammograms", Algorithms, **3**, 44-62 (2010).

[3] Llad X, Oliver A, Freixenet J, Mart R, Mart J, "A textural approach for mass false positive reduction in mammography", Computerized Medical Imaging and Graphics, **33**, 415-422 (2009).

[4] Esteve J, Kricker A, Ferlay J, Parkin D. "Facts and figures of cancer in the European Community", In: Tech. rep., International Agency for Research on Cancer, (1993).

[5] M. E. Mohamed, F. Ibrahima, B. S. Brahim, "Breast cancer diagnosis in digital mammogram using multiscale curvelet transform", Computerized Medical Imaging and Graphics, **34**, 269-276 (2010).

[6] K. Peter, P. Nikolay, "Nonlinear Operator for Oriented Texture", IEEE Transactions on Image Processing, **8**, 1395-1407 (1999).

[7] J. G. Daugman, "Two-dimensional spectral analysis of cortical receptive field profiles", Vis. Res., **20**, 847-856 (1980).

[8] S. Zehan, B. George, M. Ronald, "Monocular Precrash Vehicle Detection: Features and Classifiers", IEEE Transactions on Image Processing, **15**, 2019-2034 (2006).

[9] S. Yu, S. Shiguan, C. Xilin, G. Wen, "Hierarchical Ensemble of Global and Local Classifiers for Face Recognition", IEEE Transactions on Image Processing, **18**, 1885-1896 (2009).

[10] B. S. Manjunath, W. Y. Ma., "Texture features for browsing and retrieval of image data", IEEE Transactions on Pattern Analysis and Machine Intelligence, **18**, 837-842 (1996).

[11] S. Grigorescu, N. Petkov, P. Kruizinga, "Comparison of texture features based on Gabor filters," IEEE Transaction on Image Processing., **11**, 1160-1167 (2002).

[12] V. Vapnik, Statistical Learning Theory, Springer-Verlag, New York, NY, (1995).

[13] B. E. Boser, I. M. Guyon, V. Vapnik, "A training algorithm for optimal margin classifiers", In Proc. of the fifth annual workshop on Computational learning theory, 144-152 (1992).

[14] C. Burges, "Tutorial on support vector machines for pattern recognition", Data Mining Knowledge Discovery., **2**, 955-974 (1998).

[15] C. W. Hsu, C. C. Chang, and C. J. Lin, "A Practical Guide to Support Vector Classification", Technical report, Department of Computer Science and Information Engineering, National Taiwan University, (2010).

[16] B. Ioan, Gacsadi A., "Directional features for automatic tumor classification of mammogram images", Biomedical Signal Processing and Control, **6**, 370-378 (2011).

[17] Oliver A, Freixenet J, Mart J, et al, "A review of automatic mass detection and segmentation in mammographic images", Med. Image Anal, **14**, 87-110 (2010).

[18] Domnguez AR, Nandi AK, "Towards breast cancer diagnosis based on automated segmentation of masses in mammograms", Pattern Recognition, **42**, 1138-1148 (2009).

[19] Tang J, Rangayyan RM, Xu J, et al, "Computer-aided detection and diagnosis of breast cancer with mammography: recent advances", IEEE T Inform Techn in Biomed, **13**, 236-251 (2009).

[20] Elter M, Horsch A, "CADx of mammographic masses and clustered micro calcifications: a review", Med Phys, **36**, 2052-2068 (2009).

[21] Szkely N, Tth N, Pataki B, "A hybrid system for detecting masses in mammographic images", IEEE T Instrum Meas, **55**, 944-952 (2006).

[22] Y. Wang, X. Gao, J. Li, in, "A Feature Analysis Approach to Mass Detection in Mammography Based on RF-SVM", ICIP07, 9-12 (2007).

[23] A. P. Nunes, A. C. Silva, A. C. de Paiva, "Detection of masses in mammographic images using geometry, Simpson's Diversity Index and SVM", Int. J. Signal Imaging Syst. Eng., **3**, 43-51 2010.

[24] Wei D, Chan H, Helvie M, Sahiner B, Petrick N, Adler D, Goodsitt M, "Classification of mass and normal breast tissue on digital mammograms: Multiresolution texture analysis", Medical Physics, **22**, 1501-1513 (1995).

[25] W. B. Sampaio, E. M. Diniz, A. C. Silva,A. C. Paiva, M. Gattass, "Detection of masses in mammogram images using CNN, geostatistic functions and SVM", Computers in Biology and Medicine, **41**, 653-664 (2011).

[26] M. R. Turner, "Texture Discrimination by Gabor functions", Biological Cybernetics, **55**, 71-82 (1986).

[27] Bhangale, T., Desai, U.B., Sharma U, "An unsupervised scheme for detection of microcalcifications on mammograms", In Proc. of IEEE Int. Conf. on Image Proc., Vancouver, BC, Canada, 184-187 (2000).

[28] Rogova G. L., Stomper P. C., Ke C, "Microcalcification texture analysis in a hybrid system for computer aided mammography", Proc. SPIE, 1426-1433 (1999).

[29] S. Lahmiri, M. Boukadoum, "Hybrid Discrete Wavelet Transform and Gabor Filter Banks Processing for Mammogram Features Extraction", Proc. NEWCAS, France, IEEE Computer Society, 53- 56 (2011).

[30] D. D. Costa, L. F. Campos and A. K. Barros, "Classification of breast tissue in mammograms using efficient coding", Bio-Medical Engineering, On-Line, 2011, 10:55, http://www.biomedical-engineering-online.com/content/10/1/55.

[31] Geraldo Braz Junior et. al., "Classification of breast tissues using Moran's index and Geary's coefficient as texture signatures and SVM", Comp. in Bio and Med., **39**, 1063-1072 (2009).

[32] Heath M., Bowyer K., Kopans D., Moore R., Kegelmeyer P.J. "The digital database for screening mammography", Int. Work. Dig. Mamm., 212-8 (2000).

[33] Defeng Wang, Lin Shi, Pheng A. Heng, "Automatic detection of breast cancers in mammograms using structured support vector machines", Neurocomputing, **72**, 3296-3302 (2009).

[34] Fatemeh Moayedi et. al., "Contourlet-based mammography mass classification using the SVM family", Comp. in Bio. and Med., **40**, 373-383 (2010).

[35] Garca S, Herrera F, "An extension on "Statistical Comparisons of Classifiers over Multiple Data Sets" for all pairwise coparisons", Mach Learn Res., **9**, 2677-2694 (2008).

[36] J. Demsar, "Statistical Comparisons of Classifiers over Multiple Data Sets", Machine Learning Research, **7**, 1-30 (2006).

Muhammad Hussain is an Associate Professor in the Department of Computer Science, King Saud University, Saudi Arabia. He received both his M.Sc. and M.Phil., from University of the Punjab, Lahore, Pakistan, in 1990 and 1993 respectively. In 2003, He received a Ph.D. in Computer Science, specializing in Computer Graphics from Kyushu University, Fukuoka, Japan. He worked as a researcher at Japan Science and Technology Agency from April 2003 to September 2005. In September 2005, he joined King Saud University as an Assistant Professor. He worked on a number of funded projects in Kyushu University, Japan and King Saud University, Saudi Arabia. His current research interests include multiresolution techniques in Computer Graphics and Image Processing.

Salabat Khan received the BS. degree in computer science from Virtual University of Pakistan, in 2007 and the MS. degree in computer science from FAST - National University of Computer and Emerging Sciences, in 2009 and awarded with Gold Medal as an indication of distinction. He is currently working toward the Ph.D. in degree of computer science at the FAST - National University of Computer and Emerging Sciences. His current research interests include data mining, pattern analysis, medical images processing, bio-informatics and all kinds of bio-inspired algorithms (mainly, evolutionary and swarm based algorithms and in particular, ant colony algorithms).

Ghulam Muhammad received his Bachelor degree in Computer Science and Engineering from Bangladesh University of Engineering and Technology in 1997, and M.E. and Ph.D. degrees in 2003 and 2006, respectively, from Toyohashi University of Technology, Japan. After serving as a JSPS (Japan Society for the Promotion of Science) fellow, he joined as a faculty member in the College of Computer and Information Sciences at King Saud University, Saudi Arabia. His research interests include digital signal processing, automatic speech recognition, and multimedia forensics.

Iftikhar Ahmad received the B.Sc. degree in Mathematics and Physics from Islamia University, Bahawalpur, Pakistan, in 1999 and the M.Sc. Computer Science from University of Agriculture, Faisalabad, Pakistan in 2001. He obtained his MS/M.Phil degree in Computer Science from COMSATS Institute of Information Technology, Abbottabad, Pakistan in 2007. He received the Ph.D. degree in Information Technology from Universiti Teknologi PETRONAS, Malaysia. He has published several papers in highly reputed international conferences and journals. His research interests include Soft Computing, Network Security, Intrusion Detection, Analytic Hierarchy Process, and C4I systems.

George bebis received his BS degree in Mathematics from the University of Crete in 1987, the MS degree in Computer Science from the University of Crete in 1991, and the PhD degree in Electrical and Computer Engineering from the University of Central Florida in 1996. He is currently a Professor in the Department of Computer Science and Engineering at the University of Nevada, Reno (UNR), director of UNR's Computer Vision Laboratory (CVL), and Visiting Professor at King Saud University. Prior to joining UNR, he was a Visiting Assistant Professor in the Department of Mathematics and Computer Science at the University of Missouri-St. Louis (UMSL).